Investigating a coaxial linear microwave

IOP PUBLISHING JOURNAL OF PHYSICS D: APPLIED PHYSICS

J. Phys. D: Appl. Phys. **44** (2011) 385202 (9pp) doi:10.1088/0022-3727/44/38/385202

Investigating a coaxial linear microwave discharge

S Hübner, J Wolthuis, J M Palomares, J J A M van der Mullen

Department of Applied Physics, Eindhoven University of Technology, PO Box 513, 5600 MB Eindhoven, The Netherlands

E-mail: S.Huebner@tue.nl and J.J.A.M.v.d.Mullen@tue.nl

Received 6 April 2011, in final form 12 July 2011
Published 5 September 2011
Online at stacks.iop.org/JPhysD/44/385202

Abstract

Microwave discharges with powers around 120 W at $f = 2.45$ GHz created in low pressure argon gas at 0.1–3 mbar were investigated. The microwave energy is fed into a coaxial structure with the plasma as the outer conductor in such a way that a spatially extended surface wave was created. This linear geometry is advantageous for large area plasma processes. The discharge itself was examined spatially resolved by several kinds of optical emission spectroscopic methods. The absolute line intensity of argon 4p levels was measured and the electron temperature could be determined from this with the help of a collisional radiative model. Additionally, the absolute continuum radiation intensity method was employed to determine the electron density.

(Some figures in this article are in colour only in the electronic version)

1. Introduction

Low pressure plasmas are widely and successfully employed for the activation, coating, etching and other surface treatments of many types of materials. Due to the large variety of surface modifications that can be obtained and because of the environmental aspects, there is a rapidly growing interest in this field. Of special interest are high-frequency (HF) plasmas. They are advantageous for several applications in comparison with glow or low frequency discharges. The major difference is that HF discharges can be constructed without a plasma–electrode interaction and without the biasing of substrates. Since that is a highly desirable aspect, HF plasmas are used in a wide range of applications especially for delicate surfaces.

We intend to focus on microwave-induced plasmas (MIP), i.e. discharges excited by electromagnetic fields with frequencies in the range 300 MHz–300 GHz. Plasmas created by microwaves usually contain higher electron densities than their RF equivalent, providing more energy for activation and reactions without higher gas temperatures. The generators with the frequency of 2.45 GHz are inexpensive and therefore widely used in several kinds of plasma sources. One distinguishes between torches, cavities and surface wave sustained discharges, which can be operated under various circumstances that can be obtained by changing the pressure, geometry and fill chemistry.

To have scalable and efficient applications it is necessary to create a spatially extended, homogeneous microwave plasma. Surface wave sustained discharges offer a promising solution. Several plasma sources are known such as the surfatron/surfaguide or slotted-line antennas. The source dealt with in this study is a coaxial transmission line in which the plasma is the outer conductor. This forces the microwaves to form solutions which can be described as in a shielded surfatron 'inside–out', because in this structure the interface plasma–dielectric is positioned inverse to the arrangement found in a normal surfatron with a metal screen. A quartz tube filled with air at atmospheric pressure encloses the antenna so that the plasma is not in contact with the antenna. The advantage of a greater plasma volume than in the case of a surfatron is combined with the possibility to treat surfaces remotely. That leads to applications such as large area plasma depositing for thin film solar cells [1] or decontamination of heat sensitive surfaces [2]. For an overview of applications and a more detailed description of this kind of plasma source see [3–8]. Also models were employed to describe these plasma sources [9, 10].

Investigations of the basic plasma properties of this kind of sources, such as the electron density n_e and temperature T_e, were performed by, e.g., Letout *et al* [7]. They determined spatially resolved measurements using the Langmuir probe

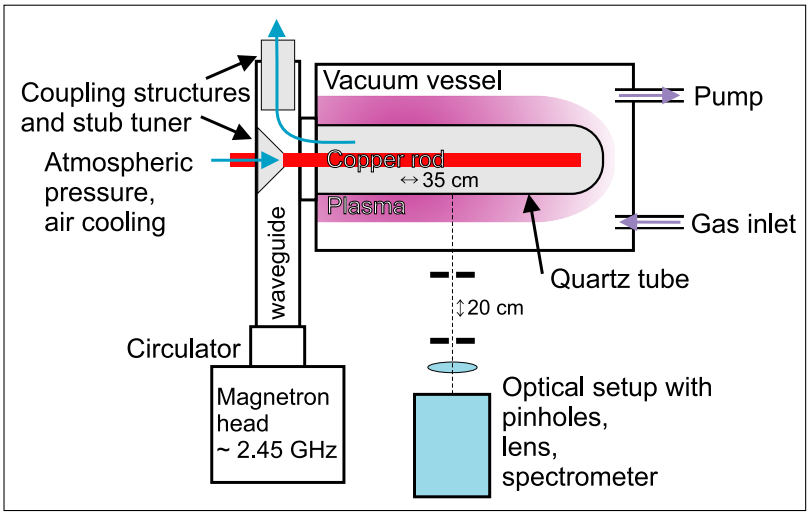

Figure 1. Scheme of the setup, note that rod structure does not reach the opposite wall; as the latter situation is often found in industrial applications.

method and optical emission spectroscopy. Apart from that, power measurements on the switching behaviour of these discharges were performed by Petasch and coworkers. While the application of probes is limited to very low pressures to our knowledge n_e and T_e have not been measured at higher gas pressures. As a first step we therefore applied passive emission spectroscopy on an argon plasma of typical 1 mbar, powered by 120 W in a coaxial plasma source. The length of the plasma was about 40 cm and the radial extension around 1 cm.

One focus in this study is the determination of the radial electron density profile. For this purpose the absolute continuum intensity (ACI) method was used. For an overview and the basic assumptions of this technique see [11–16]. The amount of continuous light radiating from a certain volume can be related to bremsstrahlung. In our study that is mainly generated by electron–atom interactions. The emission of bremsstrahlung is energy dependent and although this dependence is a rather weak function for the temperature range of low pressure microwave plasmas ($T_e = 1$–4 eV), we have to take this into account. Consequently the second focus of this study is to determine T_e. We used the absolute line intensity (ALI) method [17]. The emission of several argon lines was measured absolutely, preferably originating from a broad variety of different excited states. From that we could determine the occupation of the emitting states. When plotting these in a Boltzmann plot one obtains so-called spectroscopic temperatures. Temperatures in plural, because for the type of plasmas under study, the result depends on the excitation energy and on the departure of the plasma from equilibrium. A technique was applied to correct for that deviation. Taking a collisional radiative (CR) model with a certain electron density and temperature as a first assumption, one can calculate the deviation from partial Boltzmann equilibrium. This leads to an electron temperature which then improves the accuracy of the CR-model. That was done iteratively until convergence was reached. Applying that to the plasma, both parameters were obtained via absolute intensity measurements (AIM). Under typical conditions n_e reaches values of 1.8×10^{19} m^{-3} increasing with gas pressure and input power, whereas T_e was found to be about 1 eV; it slightly decreases with increasing gas pressure. Both values have typical error margins of about 10%.

2. Experimental setup

The setup is schematically shown in figure 1. A microwave generator (Muegge, nominal power 1.2 kW) generates microwaves at 2.45 GHz. The electromagnetic waves are coupled into a waveguide and pass a circulator to prevent the back reflection that might damage the generator. Subsequently the microwaves pass a structure designed to couple the TE_{10} mode waves from a rectangular hollow conductor into a coaxial conductor and a TM_{0n} mode. The coaxial structure has no outer conductor in the vacuum vessel. The inner hollow rod (copper, outer diameter 8 mm), which is centred in the vessel serves as an antenna for microwaves. Around the rod a cylindrical shaped dielectric tube is placed (quartz, outer diameter 30 mm), filled with air at atmospheric pressure. A flow is applied to cool the quartz tube and the coupling waveguide parts. The plasma is ignited around this quartz tube. As a function of the gas pressure and input power the discharge covers the tube length partly or completely. It has to be added here that the microwave power given in the following is always the input power leaving the generator. An unknown amount of energy is dissipated in the wave path. It is reflected and damped on edges and on the coupling parts. On similar setups one can find losses up to 30%.

The vacuum system itself consists of a stainless steel vessel as outer containment. Therefore, the vacuum confinement is accomplished by the quartz tube and the vessel. A root pump and valves ensure a working pressure in the plasma vessel of around 1 mbar, while the pre-vacuum pressure reaches down to 0.01 mbar. Different working gases can be fed into the vessel.

To investigate this plasma source an optical setup was built. The light created by the plasma passes a glass window. Afterwards it is collected through a combination of

two pinholes, optional interference filters and a collimating lens. Behind that, the spectral detection is performed either with a low resolution spectrometer (OceanOptics 2000P) for the continuum emission or a high resolution spectrometer (DEMON, Lasertechnik Berlin) for the line intensities. By this arrangement we measured with a spatial resolution of less than 1 mm. The emission was calibrated with a tungsten ribbon lamp. The ribbon was placed at the same distance from the spectrometer as the plasma. Moreover, the absorption of the window, the lenses and the interference filter were measured separately.

3. Optical emission diagnostics

In this study we measure lines and continuum emission from the plasma. The lines arise from electronic transitions between bound states, whereas the continuum is created by interactions of free particles. Since the plasmas under study are optically thin for the radiation of interest, the transport equation becomes

$$\frac{\mathrm{d}I_\lambda(\lambda)}{\mathrm{d}s} = j_\lambda(\lambda), \tag{1}$$

which describes the increase in the spectral intensity $I_\lambda(\lambda)$ in $\mathrm{W\,m^{-2}\,sr^{-1}\,nm^{-1}}$ along its path through a medium due to the source given by j_λ, the emission coefficient ($\mathrm{W\,m^{-3}\,sr^{-1}\,nm^{-1}}$). Every laboratory plasma has boundaries that change the emission at the edge. However, assuming a homogeneous plasma along the line of sight D, we can write

$$I_\lambda(\lambda) = j_\lambda(\lambda) D. \tag{2}$$

If the plasma is cylindrically symmetric we can use an inverse Abel transformation to deduce local values of the emission coefficient from the lateral distribution of the intensity. As we will show later this is used in this study in a simplified way.

3.1. Absolute continuum method

The full ACI method uses the continuous emission generated by electron–atom and electron–ion interactions. By doing absolute continuum measurements the electron density n_e can be determined, since the measured signal depends directly on the number density of the interactions, and thus on the product of the densities of the interacting species. The continuum emission is composed of three contributions: the free-bound recombination radiation of electrons with ions $j_\lambda^{\mathrm{ei,fb}}(\lambda)$, the free–free bremsstrahlung created by electron–ion interactions $j_\lambda^{\mathrm{ei,ff}}(\lambda)$ and the free–free radiation created by electron–atom interactions $j_\lambda^{\mathrm{ea,ff}}(\lambda)$. We can thus write

$$j_\lambda(\lambda) = j_\lambda^{\mathrm{ei,fb}}(\lambda) + j_\lambda^{\mathrm{ei,ff}}(\lambda) + j_\lambda^{\mathrm{ea,ff}}(\lambda). \tag{3}$$

To describe the free–free electron–atom radiation we start with the expression

$$j_\lambda^{\mathrm{ea,ff}}(\lambda) = \mathrm{const} \cdot \frac{n_\mathrm{e} n_\mathrm{a}}{\lambda^2} \int_{E_0}^{\infty} Q_{\mathrm{BS}}(E) \sqrt{E} f(E)\,\mathrm{d}E \tag{4}$$

that is based on the collision integral of the interacting species. For the cross section for bremsstrahlung there exist several approaches, such as the expression

$$Q_{\mathrm{BS}} = \mathrm{const} \cdot \left(2 - \frac{hc}{\lambda E}\right) \cdot \sqrt{1 - \frac{hc}{\lambda E}} \cdot Q_{\mathrm{mom}} \tag{5}$$

given by Kas'yanov and Starostin [18]. However, the rate of interactions depicted by the integral in equation (4) is then difficult to solve. A common approach is to treat the problem like elastic collisions [15]

$$Q_{\mathrm{BS}}(E) = \mathrm{const} \cdot Q_{\mathrm{mom}}(E). \tag{6}$$

Where Q_{mom} is the cross section for elastic momentum transfer collisions of electrons with atoms. Moreover, one can assume an energy averaged cross section $\langle Q_{\mathrm{mom}}(T_\mathrm{e})\rangle$. That is based on the observation that Q_{BS} is only a weakly varying function of the energy [18]. We refer to [12, 13, 15, 16, 18, 19] for more details of the derivations. We will follow the latter approach of elastic collisions, that will enable us to have an energy independent cross section based on the momentum transfer cross section. Moreover, in the integration of (4) a Maxwellian energy distribution of the electrons $f(E) = \mathrm{Maxwell}(T_\mathrm{e})$ is assumed. The lower energy boundary E_0 corresponds to the minimum energy that an electron needs to have in order to generate a photon with the requested wavelength $\lambda = hc/E_0$. Using $\langle Q_{\mathrm{mom}}(T_\mathrm{e})\rangle$ we can write $j_\lambda^{\mathrm{ea,ff}}$ as follows

$$j_\lambda^{\mathrm{ea,ff}} = c_{\mathrm{ea}} \frac{n_\mathrm{e} n_\mathrm{a}}{\lambda^2} T_\mathrm{e}^{3/2} \langle Q_{\mathrm{mom}}(T_\mathrm{e})\rangle \left(1 + \left(1 + \frac{hc}{\lambda k_\mathrm{B} T_\mathrm{e}}\right)^2\right) \times \exp\left(-\frac{hc}{\lambda k_\mathrm{B} T_\mathrm{e}}\right). \tag{7}$$

Where we use for the cross section Q_{mom} the widely accepted formula determined by Phelps *et al* [20]. Furthermore T_e is the electron temperature, k_B the Boltzmann constant, h Planck's constant and c_{ea} a constant, defined as

$$c_{\mathrm{ea}} = \frac{e^2 k_\mathrm{B}^{3/2}}{3c^2 \epsilon_0 m_\mathrm{e}^{3/2} \pi^{5/2}} = 1.026 \times 10^{-34}\ (\mathrm{J m^4\,K^{3/2}\,s^{-1}\,sr^{-1}}). \tag{8}$$

The emission coefficient of the other two contributions, $j^{\mathrm{ei,ff}}$ and $j^{\mathrm{ei,fb}}$, can be incorporated into one expression

$$j_\lambda^{\mathrm{ei,ff+fb}} = c_{\mathrm{ei}} \frac{n_\mathrm{e} n_\mathrm{i}}{\lambda^2} T_\mathrm{e}^{-1/2} \left\{ \left(1 - \exp\left(-\frac{hc}{\lambda k_\mathrm{B} T_\mathrm{e}}\right)\right) \xi_{\mathrm{fb}}(\lambda, T_\mathrm{e}) + \left(\exp\left(-\frac{hc}{\lambda k_\mathrm{B} T_\mathrm{e}}\right)\right) \xi_{\mathrm{ff}}(\lambda, T_\mathrm{e}) \right\}. \tag{9}$$

The prefactor equals $c_{\mathrm{ei}} = 1.68 \times 10^{-43}\,\mathrm{J m^4\,K^{3/2}\,s^{-1}\,sr^{-1}}$. The $\xi(\lambda, T_\mathrm{e})$'s are known as the Biberman-coefficients. They represent the non-hydrogenic behaviour of the electron–ion interaction, and are therefore ion specific [21, 22]. We introduce a combined Biberman-coefficient ξ_{tot} given by the expression

$$\xi_{\mathrm{tot}} = \left(1 - \exp\left(-\frac{hc}{\lambda k_\mathrm{B} T_\mathrm{e}}\right)\right) \xi_{\mathrm{fb}}(\lambda, T_\mathrm{e}) + \left(\exp\left(-\frac{hc}{\lambda k_\mathrm{B} T_\mathrm{e}}\right)\right) \xi_{\mathrm{ff}}(\lambda, T_\mathrm{e}). \tag{10}$$

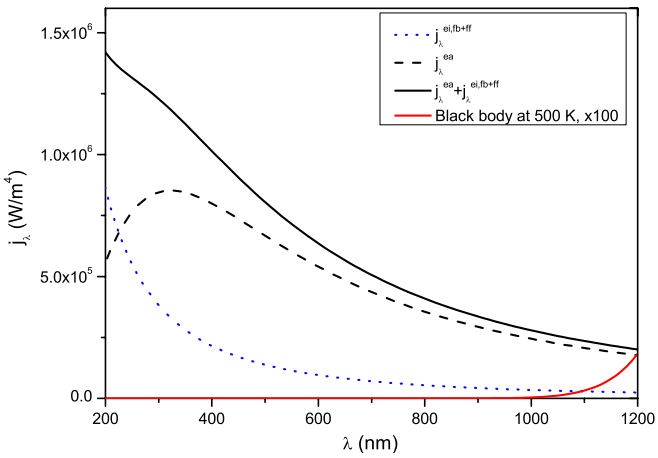

Figure 2. Different contributions to continuum radiation in an argon plasma as a function of the wavelength, calculated for $n_a = 1.5 \times 10^{22}$ m^{-3}; $T_e = 1.1$ eV and $n_e = 10^{19}$ m^{-3}. In the visible range the dominant contribution is that generated by electron–atom bremsstrahlung. Note that ξ_{tot} (see equation 10) is taken constant which is only true in the visible wavelength range and for $T_e = 0.5$–2 eV.

This ξ_{tot} is fairly constant for the visible range of emitted wavelength and also in the temperature range of the microwave plasma under study. By taking it constant and equal to 1.3 we make an error of 5% [16] in the T_e range 0.5–2 eV. To simplify expressions (7) and (9) we introduce the functions $f_\lambda(\lambda, T_e)$ and $g_\lambda(\lambda, T_e)$ such that we can write

$$j_\lambda^{ei,fb}(\lambda) + j_\lambda(\lambda)^{ei,ff} = (n_e)^2 f_\lambda(\lambda, T_e), \tag{11}$$

$$j_\lambda^{ea,ff}(\lambda) = (n_e n_a) g_\lambda(\lambda, T_e). \tag{12}$$

The cross section for electron–ion interactions creating emission is larger than for electron–atom interactions in the T_e-range of interest. However, the ionization degree is with $n_e/n_a \approx 6 \times 10^{-4}$ so low that the electron–atom interactions give the most important contribution to the continuum as can be seen in figure 2. This is an important fact, since it is in contrast to many plasmas being studied, such as arcs, shock tubes or most astrophysical plasmas. However, at a wavelength of 580 nm the electron–ion interactions contribute with a fraction of about 24% to the continuum, so that in contrast to the study of Iordanova *et al* [16] the electron–ion interactions cannot be neglected. Using formule (11) and (12) we get the following expression for the electron density:

$$n_e = \frac{g_\lambda n_a}{2 f_\lambda}\left(\sqrt{1 + \frac{4 j_\lambda^{measured} f_\lambda}{(g_\lambda n_a)^2}} - 1\right). \tag{13}$$

The function-values of f_λ and g_λ are based on the electron temperature as found with the ALI method described in the next section.

3.2. Absolute line intensity method

Absolute optical emission spectroscopy enables us to determine the population of excited states. This makes it possible to construct the atomic state distribution function (ASDF). The idea is that we first apply the calibration per wavelength interval and than take the spectral area of the intensity corresponding to one atomic transition, that is $I_{ij} = \int_{i-j} I_{ij,\lambda} d\lambda$. The emitting density n_i can be described by

$$n_i = \frac{I_{ij} \lambda_{ij} 4\pi}{hc A_{ij} D}, \tag{14}$$

where A_{ij} denotes the Einstein coefficient for spontaneous emission and D the length of the line of sight. If the densities of the atomic states per statistical weight are ruled by the Boltzmann law, we can write

$$\eta_i = \frac{n_i}{g_i} = \frac{n_0}{g_0} \exp^{-\frac{E_i}{k_B T_e}} \tag{15}$$

where η_i is the density per statistical weight, n_0 refers to the density of the ground state, $g_{0,i}$ to the degeneracy of the corresponding level and E_i to the excitation energy. Combined with equation (14) this leads to the following expression for the electron temperature

$$\frac{E_i}{k_B T_e} = \ln\left(\frac{hc A_{ij} g_i D_i}{I_{ij} \lambda_{ij} 4\pi}\right) + \ln(\eta_0). \tag{16}$$

This equation is the basis of the Boltzmann plot method. It suggests that by presenting the densities in a semi-log plot versus the excitation energy we can obtain the temperature from the slope of the graph. However, an essential question is in how far the ASDF of our low density plasma obeys the Boltzmann law, or better follows the Boltzmann–Saha distribution. If for all excited states the number of ionization processes equals that of the corresponding reverse process of two-electron recombination, we have the Saha–Boltzmann equilibrium. The corresponding ASDF is depicted by the upper line given in figure 3. However, in the low pressure discharge electron–ion pairs will diffuse to the wall where they recombine. For the plasma volume this means that the ionization processes are not compensated anymore by two-electron recombination. Instead a process known as ladder-climbing ionization must be present to support the generation and efflux of electron–ion pairs. This demands another ASDF-shape which, instead of being constant in slope, will gradually change in shape. This is schematically given by the dashed line in figure 3 that anticipates on the measured ASDF given in figure 6.

In our case the observable excited states do not follow the distribution that corresponds to the Saha–Boltzmann equilibrium. The deviation of the local Saha equilibrium (LSE) as caused by the efflux of electron–ion pairs is manifested in the shape of the ASDF which, being variable in shape, cannot provide the electron temperature. The variable slope is sometimes expressed in a slope temperature but it has no thermodynamic meaning in the sense of being the mean energy of a group of species. In fact it can be derived that the slope of the ASDF at the location p in excitation space depends mainly on the ionization potential I_p in the following way

$$1/k_B T_{slope} \approx 1/k_B T_e + 3/I_p. \tag{17}$$

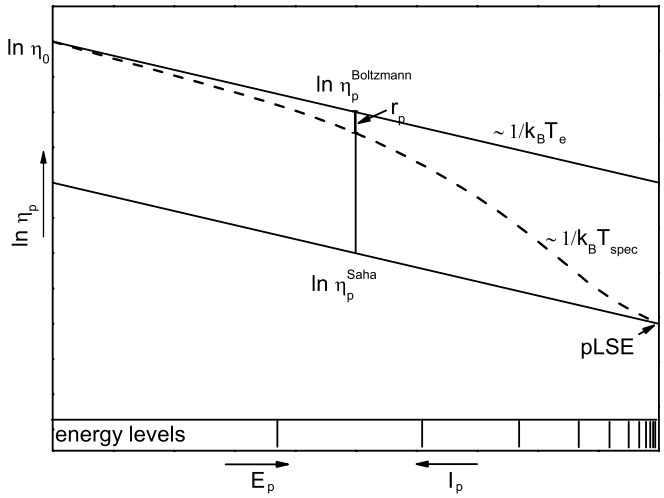

Figure 3. Schematic of a measured real ASDF (dashed) and ASDF in Saha equilibrium. This study is about ionizing systems, that means we have an overpopulation in respect to Saha to sustain the losses of electron–ion pairs. Indicated is the deviation parameter r_p to the corresponding equilibrium distribution state p.

For the whole derivation we refer to [23, 24]. To conclude the T_{slope} is only weakly influenced by T_e and it is therefore not suited for the T_e-determination. Based on the method introduced by de Vries *et al* we can use a factor r which corrects for the deviation from LSE for each level p.

$$\eta_{p,\text{real}} = \eta_0 \cdot r_p \cdot \exp \frac{-E_p}{k_B T_e}. \tag{18}$$

The 4p states can be treated as a group within an excitation energy range. This group can be detected since it radiates in the visible spectrum. The full description of the balancing processes which are needed to describe the population of that level in a CR-model is given in [17] and references therein. Based on that, we will use a value for $r_{4p} = 10^{-3}$ (r_3^1 in [17]). This corresponds to an initial assumption of the electron density and temperature. Using the measurements of the ALI and ACI methods we obtain a more precise value for r_{4p}. That procedure is done iteratively till convergence is reached. By measuring the absolute densities of the levels one can use the formula

$$\frac{E_{4p}}{\ln[(\eta_0 \cdot r_{4p})/\eta_{4p}]} = k_B T_e \tag{19}$$

to obtain the electron temperature. In our study we take 11 transitions of the argon 4p group, which are measured and averaged.

4. Results

The exploration of the experimental data starts with the study of the photograph of the plasma given in figure 4. This combined line and continuum emission will be investigated in terms of spatial emission patterns. Then the radial profile and plasma thickness is deduced from the radiation from specific atomic argon transitions. Subsequently we measure several transitions absolutely to obtain the T_e. Finally with the continuum emission the electron density is determined.

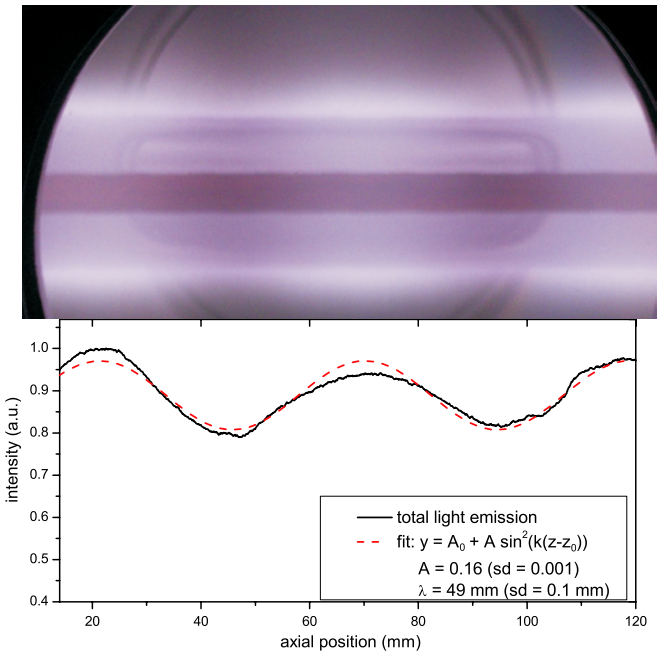

Figure 4. Upper part: picture of the discharge with its centred conducting rod surrounded by an air filled quartz tube. The discharge is burning on the outside of the quartz tube. Lower part: emission data taken from the picture and corresponding fit in the axial direction; a reason for the disagreement between the measurement and the fitting curve can be the lower reflectivity of the backside of the vessel in the centre.

4.1. Line emission pattern

In the picture of the plasma in figure 4 we observe the discharge side-on through a window in the vessel. On the backside we can see the opposite window covered by a bare metal flange. In the centre the copper rod enclosed in a quartz tube is located surrounded by a purple discharge. The discharge shows an axial wavy emission pattern. Since a standard camera picture of this argon discharge is strongly dominated by line emission, we can deduce that it is a representative image of line emission. The lateral emission close to the quartz tube was recorded as a function of the axial position. The result is shown in the lower part of figure 4. The applied microwave frequency is 2.45 GHz, which corresponds to a wavelength of $\lambda^0_{\text{mw}} = c/f = 122\,\text{mm}$ in free space. We assume that the microwaves are being reflected inside the vessel creating a standing wave. This is possible since the antenna ends inside the vessel. This is in contrast to the setups of Letout *et al* and Soppe *et al*. This could explain why they do not observe a standing wave pattern [1, 7]. The signal was fitted with a sine square function $y = A_0 + A(\sin^2(kz))$. The modulation depth is about $A/A_0 = 16\%$. The fitting depicts a standing wave with a wavelength of $\lambda = \pi/k$. The wavelength found by fitting the standing pattern is $\lambda_{\text{mes}}/2 = 49 \pm 0.1\,\text{mm}$, i.e. less than λ^0_{mw}. The difference between λ_{mes} and λ^0_{mw} can be explained by the dispersion of the propagating wave. For instance for a simple plasma–dielectric interface the wavenumber k of a propagating electromagnetic wave with the angular frequency ω depends on the relative permittivities ϵ_p and ϵ_g of the mediums (plasma and dielectric) in such a way that $k^2c^2 = \omega^2 \cdot \frac{\epsilon_p \epsilon_g}{\epsilon_p + \epsilon_g}$ [25].

Since ϵ_p is a function of n_e, the wavenumber at a fixed ω depends on n_e. This dispersion relation was evaluated for a comparable coaxial structure including electron collisions for various conditions in [26, 27]. Their results show good agreement with our wavelength obtained from the standing wave pattern. Moreover, it was observed that changing the power and therefore the electron density (see next section) increases the wavelength slightly, which is in agreement with [26]. Therewith we have a simple technique to determine n_e just by analysing the optical emission standing waves if the corresponding dispersion relation is known. We also observe a decrease in the intensity in the axial direction away from the inlet microwave structure. That is about 1% per 4 cm. This linear decreasing trend from the launching side is well known for similar plasma sources like the surfatron.

4.2. Radial emission profiles

The goal is to get a description of the radial distribution of n_e and T_e. This goes along with the determination of the radial values of the emission coefficients $j(r)$. The $n_e(r)$ is based on the $j(r)$ value of the continuum (ACI method); for the $T_e(r)$ we need the transition integrated emission coefficients of the line radiation emitted by the 4p levels (ALI method).

To deduce the radial distribution of $j(r)$ we need an Abel inversion procedure of the lateral intensity $I(x)$ profiles. However, due to the differential nature of such a procedure the result will be very sensitive to the scattering that is present in the lateral data. This scatter is among others caused by the strong internal reflections of light on the vessel walls and on the tube that surrounds the antenna. Therefore we will use the following procedure.

(i) The lateral values of the intensities are smoothed.
(ii) The results are fitted to a Gaussian shape.
(iii) The Abel inversion of the Gaussian is performed.

In the latter step we can apply the well known lemma that the Abel inversion of a Gaussian is a Gaussian. The central lateral region has to be excluded from this inversion; the reason is that the antenna and tube structure spoils the central region of the $j(r)$. This means that the Abel inversion has to be confined to the outer region. The omission of the central region does not hinder the inversion of the outer region. In practice we have to exclude somewhat more than the central part as obtained by the projection of the tube. The reason is that the central tube will also influence its direct plasma environment. This is found to be especially important in the determination of the electron density.

4.3. ALI results

This section will focus on the emission of specific atomic transitions. Firstly, we present lateral resolved profiles of the argon emission line at 738.4 nm for several plasma conditions in figure 5. This corresponds to the transition $(^2P_{1/2})4p \rightarrow (^2P_{3/2})4s$. In accordance with the Abel-procedure described above, we fit a Gaussian function to the data. That is successful for all data with a determination coefficient of $R^2 > 0.95$. The idea is that successful fitting allows us to obtain radial values.

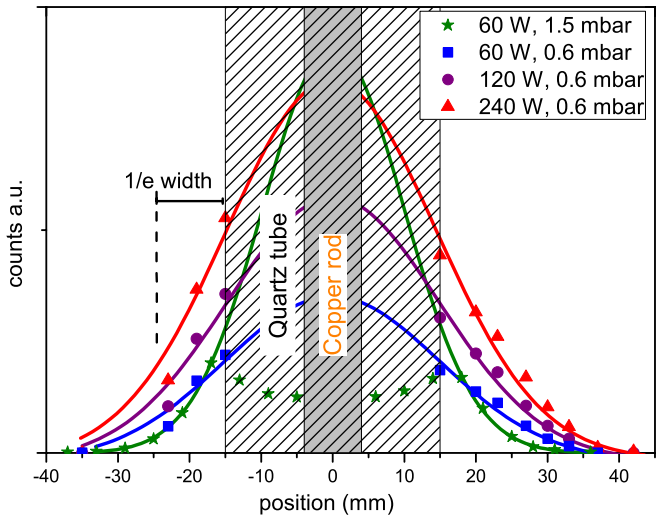

Figure 5. Lateral profiles of the emission of the argon transition at 738.4 nm taken at different plasma properties. Data points are shown by symbols, Gaussian profiles are fitted.

The width between the quartz tube and the $1/e$ value of the fitting curve was taken as the outer plasma radius R. In all further results we apply this R to correct for the line of sight length $l_m = 2R$.

Secondly, in order to obtain a T_e we apply the described ALI technique. According to the previous section we deduce T_e from the intensities of the 4p levels by correcting for the deviation from equilibrium. We measured 29 different argon emission lines in total. The intensities of these are shown absolutely calibrated on a semi-logarithmic scale for 2 different plasma conditions in figure 6. The measured 11 levels of the 4p excitation system were processed according to the deviation from Boltzmann equilibrium and averaged. The results of T_e at a distance of 1 mm from the central tube are shown in table 1. The obtained electron temperatures are in the order of 1 eV.

Despite the fact that it is very easy to measure the line intensities for the more outer regions it is not straightforward to interpret a T_e from that. The correction parameter r_{4p} (equation (18)) being rather constant for n_e values above $10^{19}\,m^{-3}$, becomes n_e-dependent for lower n_e values. This makes the iterative procedure for the outer plasma instable. That is due to the fact that lower n_e values are insufficient to establish the ladder-climbing ionization. At a constant input power we see an inverse dependence on the pressure. This trend of the plasma is understandable from the point of view of a greater demand for ionization processes if the diffusion increases, a trend triggered by the pressure decrease. It is remarkable that this can be shown in T_e even though the differences are not much. To validate this statement an error analysis and a global model calculation is performed in the next paragraphs.

With a simple global model approach the electron particle balance can be calculated. This balance is mainly determined by T_e. The ionizing reactions globally equal the diffusion losses, which can be written in the form

$$n_a k_{ion} = \frac{D_a}{\Lambda^2} \tag{20}$$

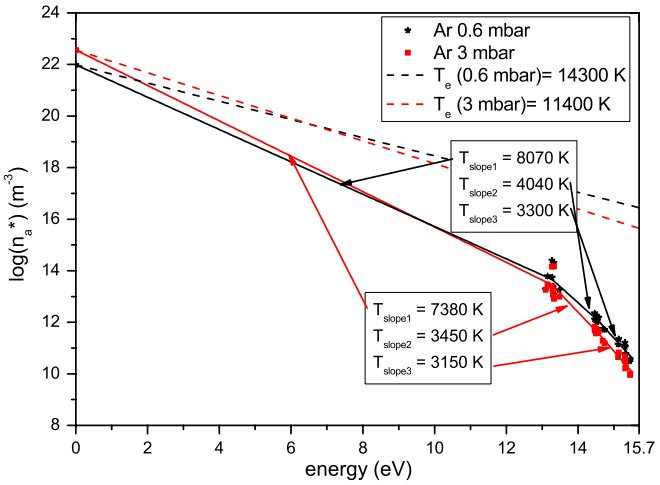

Figure 6. Absolute calibrated emission of argon transitions as a function of the energy of the emitting states for two different pressures. Indicated are three different slope (spectroscopic) temperatures T_{slope1}, T_{slope2} and T_{slope3} which can be obtained. Moreover, the distributions are shown assuming the obtained real T_{e} for both gas pressures.

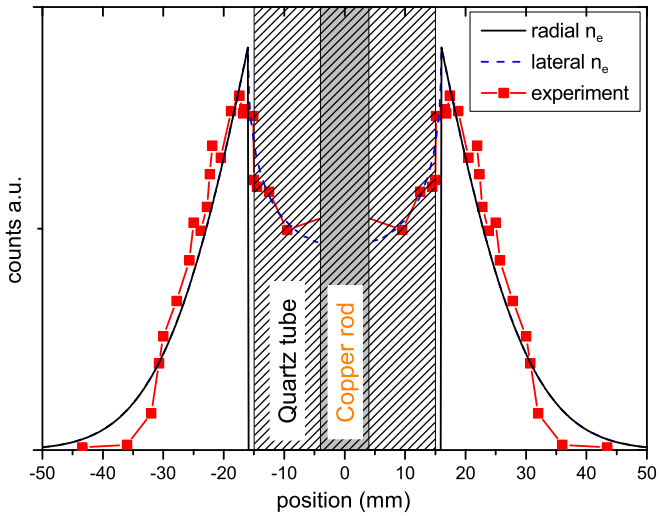

Figure 7. Calculation of the lateral projection of a radial n_{e} profile in a cylindrical symmetric geometry. Superimposed are experimental data points from continuum emission, i.e. the data points are proportional to n_{e}. See text for discussion.

Table 1. Results of T_{e} at a distance of 1 mm from the central tube.

Argon gas pressure [mbar]	Electron temperature [eV]
0.6	1.23 ± 0.1
1	1.02 ± 0.1
3	0.98 ± 0.1

where the rate coefficient for ionization is given by $k_{\mathrm{ion}} = 6.8 \times 10^{-17}\sqrt{T_{\mathrm{e}}}\cdot\exp\left(-I_{\mathrm{p}}/k_{\mathrm{B}}T_{\mathrm{e}}\right)\mathrm{m}^3\,\mathrm{s}^{-1}$. The ambipolar diffusion coefficient can be described by $D_{\mathrm{a}} = (1+T_{\mathrm{e}}/T_{\mathrm{h}})/(\sqrt{2}n_{\mathrm{a}}\sigma_{\mathrm{ai}})v_{\mathrm{th}}$. Where T_{h} is the heavy particle temperature, σ_{ai} the atom-ion momentum transfer cross section while v_{th} stands for the mean thermal velocity of the heavy particles. The diffusion length is estimated to be $\Lambda \approx 0.008\,\mathrm{m}$ based on the plasma radius. Only by changing the gas pressure from 3 mbar to 0.6 mbar (equation (20)) predicts values for $T_{\mathrm{e}} = 0.9\,\mathrm{eV}$ to 1.19 eV, respectively. That is in the scope of the rough global method a reasonable agreement with the measured data.

4.4. Error analysis of ALI

This section is devoted to the error analysis of the ALI method. Uncertainties due to different excitation–saturation processes and different transition strengths within the 4p group give rise to an error. This combines with the error in the absolute calibration, which is a function of the wavelength. That altogether makes the 4p group in figure 6 a scattered cloud. Also the uncertainty of T_{h} for the determination of the ground state density has to be taken into account. As a matter of fact T_{h} exceeds room temperature. A small addition of hydrogen gas in the discharge enables us to perform measurements of the Fulcher band emission of the hydrogen molecule. The rotational transitions of the $3p3\Pi \rightarrow 2s3\Sigma$ (Q(0-0) and Q(1-1)) in the wavelength range 600 to 630 nm were used. By making a Boltzmann plot T_{h} could be determined. That yields $T_{\mathrm{h}} = 500\,\mathrm{K}$ with a uncertainty of 10%. However, all mentioned errors account in a logarithmic form of the Boltzmann plot of the argon ASDF. Therefore they give only rise to an error of $\Delta T_{\mathrm{e}}/T_{\mathrm{e}} \leqslant 8\%$ which is one standard deviation. The systematic errors can only be guessed and therefore an uncertainty of 10% due to the whole calibration procedure was assumed. This seems rather pessimistic, but is in the authors opinion a save value.

4.5. Radial electron density profiles

The second main diagnostic method which was employed is the absolute continuum radiation method. As described above, an electron density can be deduced from the absolute emission. Again, the obtained lateral continuum emission has to be converted into local radial values. To decide whether the proposed Abel procedure is valid for the continuum emission as well, we made a simple calculation. We assume in the cylindrical symmetric setup a radial n_{e} distribution with a Gaussian shape while a circular part in the centre is omitted. When the lateral projection of this density yields a profile presented in figure 7. The emission from the lateral central part is modified by the unknown optical attenuation, distortion and reflection properties of the copper and the quartz tube. However, a fairly good fitting can be seen. In the centre of the radial profile of n_{e} we exclude a slightly bigger area than the tube dimension itself. That is justified by the experimental findings. In the vicinity of the quartz tube the losses of electrons towards the wall may alter the profile and thus the fitting yields the best results with a slightly bigger omitted part. The results for n_{e} as a function of pressure are presented in figure 8. The highest electron density was measured close to the quartz tube with about 20×10^{18}, $(14 \times 10^{18}, 8 \times 10^{18})\,\mathrm{m}^{-3}$ for pressures of 3 (1, 0.6) mbar. n_{e} decreases as a function of the distance to the tube. The radial thickness of the discharge R is between 16 and 3 mm for 0.6 to 3 mbar. Moreover, the maximum of n_{e} at about 2 (5) mm is shifted to the outer

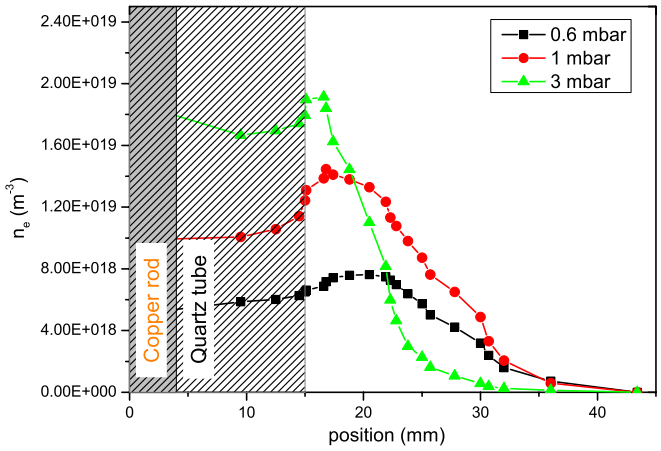

Figure 8. Shown are measurements of the lateral profile of n_e by continuum radiation taken at different argon gas pressures with an input power of 120 W. The signal is corrected for the stray light and the length of the line of sight. For the lateral outer regions we showed that the profile is very close to the radial profile, while that is not true in the central area.

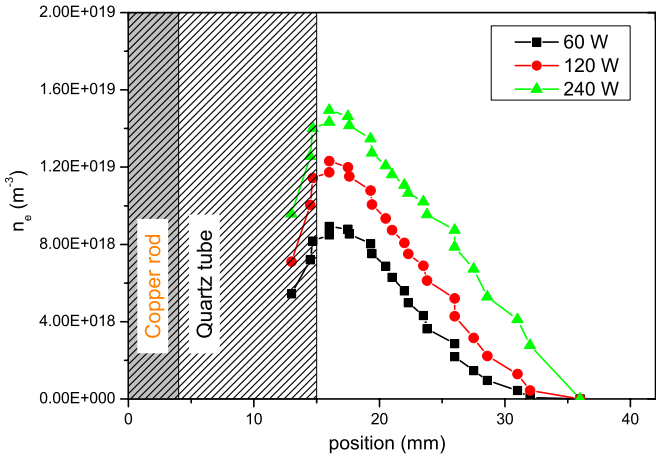

Figure 9. Measurement of the lateral profile of n_e by continuum radiation at different input powers at an argon gas pressure of 1 mbar. (see also figure 8).

region if the pressure decreases from 3 to 0.6 mm. That is an interesting finding since one can extrapolate this result to lower pressure and compare that with findings from Letout *et al* [7]. They observed the highest n_e values of about 3×10^{17} m^{-3} at a distance of 20 mm from the central tube at a gas pressure of 0.04 mbar. On the other hand the results of Petasch *et al* [5] obtained with electrical probe measurements show a systematic lower n_e value than our work with about 2×10^{17} m^{-3} under comparable plasma conditions.

We measure also the dependence of the input power as given in figure 9. It shows an increase in the electron density from 9×10^{18} to 15×10^{18} m^{-3} for an input power increasing from 60 to 240 W. From this measurement can be concluded that the width of the plasma region increases with increasing power. The $1/e$-width value changes about 30%. The radial profile seems not to change with the input power. An analytical function to describe the radial profile we propose in accordance with the Abel inversion a Gaussian shape, sparing out the central part. A more in depth numerical analysis, especially of the region close to the centred quartz tube, is limited by the size of the detection volume.

As was pointed out in the introduction the EM-waves in this plasma source behave similarly to the surface-waves sustaining the plasma in a surfatron. For a surfatron it is well known that for a sufficient high parameter $n_a R$, where R is the plasma radius, the EM-fields penetrating the plasma are strongly attenuated in the radial direction, i.e. skin effect. The same we expect for the outer region of the coaxial discharge. In fact it was verified by numerical modelling that fields penetrate only about 1 mm into the plasma [28]. It has to be noted here that solutions for the surfatron ([25] and references therein) seem to be applicable for the coaxial structure apart from the fact that the central metal rod changes the propagating modes and allows multiple modes.

In this setup the detection limit of continuum radiation is determined by the stray light level. The stray light level in respect to the continuum emission for calculation of n_e is at maximum $n_e(\text{stray})/n_e \approx 7\%$. That value depends on the pressure, power and lateral position. Hence a possible source of errors arises, since the subtracted stray light is determined by the outermost lateral observed part of the discharge, but the stray light might differ if obtained from a region laterally closer to the centre of the discharge.

5. Summary

Passive optical emission diagnostic methods were employed to determine the parameters n_e and T_e. The calibrated emission of several argon transitions was measured and the population of the emitting states was corrected for their deviation from Boltzmann equilibrium as predicted by a CR-model. Subsequently the revised distribution of the excited states gives the real electron temperature. That differs intrinsically from the spectroscopic or slope temperature which is obtained directly from the excited states distribution.

T_e is used to calculate the energy-dependent electron–atom momentum transfer cross section. After that we processed the measured continuum emission and via absolute calibration we determined the electron density. This method was developed in Iordanova *et al* for a surfatron discharge and in this study it is for the first time applied to a coaxial microwave discharge in low pressure. The results of n_e are in the order of 10^{19} m^{-3}. The plasma was confined close to the central quartz tube. For gas pressures above 3 mbar the radial profile of n_e was very similar to a Gaussian profile. These results can be seen as an extrapolation of experiments done by Letout *et al* towards higher gas pressure. They observe much less confinement of n_e and additionally higher T_e values at lower gas pressure.

It was shown that this microwave source provides high n_e values while having no plasma–electrode contact. Moreover, this plasma source is very robust in a sense that the propagation of power is sustained by the plasma and the central conducting rod. The latter can guide modes without the plasma. Combining these facts makes the plasma source suitable for applications with high requirements in terms of stability and

homogeneity. Moreover, we provide measured radial n_e profiles, e.g., for applications which are sensitive for the ionization degree.

Simple and non-disturbing methods enable us to obtain a quite precise picture of the plasma properties. For that it is crucial to know how far the plasma is out of equilibrium. To validate and calibrate these measurements, laser scattering experiments as well as numerical models are planned for the future.

Acknowledgments

This work is supported by the Dutch Technology Foundation (STW project 10497) and the Energy Research Centre of the Netherlands (ECN).

References

[1] Soppe W, Rieffe H and Weeber A 2005 *Prog. Photovolt: Res. Appl.* **13** 551–69
[2] Ehlbeck J, Ohl A, Maaß M, Krohmann U and Neumann T 2003 *Proc. 8th Int. Conf. Plasma Surf. Eng. (Garmisch Partenkirchen, Germany 9–13 September 2002) Surf. Coat. Technol.* **174–175** 493–7
[3] Ehlbeck J, Schnabel U, Polak M, Winter J, von Woedtke Th, Brandenburg R, von dem Hagen T and Weltmann K-D 2011 *J. Phys. D: Appl. Phys.* **44** 013002
[4] Liehr M and Dieguez-Campo M 2005 *Surf. Coat. Technol.* **200** 21–5
[5] Petasch W, Räuchle E, Muegge H and Muegge K 1997 *Surf. Coat. Technol.* **93** 112–8
[6] Walker M, Baumgärtner K-M, Feichtinger J, Kaiser M, Schulz A and Räuchle E 2000 *Vacuum* **57** 387–97
[7] Letout S, Alves L L, Boisse-Laporte C and Leprince P 2005 *J. Optoelectron. Adv. Mater.* **7** 2471–5
[8] Boisse-Laporte C, Leroy O, de Poucques L, Agius B, Bretagne J, Hugon M C, Teulé-Gay L and Touzeau M 2004 *Surf. Coat. Technol.* **179** 176–81
[9] Alves L L, Letout S and Boisse-Laporte C 2009 *Phys. Rev.* E **79** 016403
[10] Alves L L, Gousset G and Ohl A (ed) 2003 *INP Greifswald* Germany
[11] Delgarno A and Lane N F 1966 *Astrophys. J.* **145** 623
[12] Lawler J E 2004 *J. Phys. D: Appl. Phys.* **37** 1532–6
[13] Burm K T A L 2004 *Plasma Sources Sci. Technol.* **13** 387–94
[14] Chapelle J and Cabannes F 1969 *J. Quant. Specrosc. Radat. Transfer* **9** 889–919
[15] Cabannes F, Chapelle J C and Venugopalan M (ed) 1976 *Spectroscopic Plasma Diagnostics Reaction Under Plasma Conditions* (New York: Wiley)
[16] Iordanova E, de Vries N, Guillemier M and van der Mullen J J A M 2008 *J. Phys. D: Appl. Phys.* **41** 015208
[17] de Vries N, Iordanova E, Hartgers A, van Veldhuizen E M, van den Donker M J and van der Mullen J J A M 2006 *J. Phys. D: Appl. Phys.* **39** 4194–203
[18] Kas'yanov V and Starostin A 1965 *Sov. Phys.—JETP* **48** 295–302
[19] Pfau S, Rutscher A and Winkler R 1976 *Beitr. Plasmaphys.* **16** 317–22
[20] Phelps A V and Petroviĉ Z Lj 1999 *Plasma Sources Sci. Technol.* **8** R21–44
[21] Schlüter D 1987 *Z. Phys. D: Appl. Phys.* **6** 249–54
[22] Biberman L M and Norman G E 1967 *Sov. Phys.—Usp.* **10** 52
[23] Jonkers J and van der Mullen J J A M 1999 *J. Quant. Specrosc. Radat. Transfer* **61** 703–9
[24] van der Mullen J J A M 1990 *Phys. Rep.* **191** 109–220
[25] Schlüter H and Shivarova A 2007 *Phys. Rep.* **443** 121–255
[26] Letout S 2007 Couplage onde de surface-plasma en présence de résonance, dans une décharge micro-onde à basse pression *PhD Thesis* Université Paris-Sud, France
[27] Nie Z, Liu F, Zhou Q, Chang X, Zhang S and Liang R 2009 *Europhys. Lett.* **86** 35001
[28] Diaz M J 2011 private communication